IIE Transactions (2012) **44**, 534–550

ISSN: 0740-817X print / 1545-8830 online
DOI: 10.1080/0740817X.2011.596509

Statistical characterization of nanostructured materials from severe plastic deformation in machining

MARCUS B. PERRY[1], JEFFREY P. KHAROUFEH[2,*], SHASHANK SHEKHAR[2], JIAZHAO CAI[2] and M. RAVI SHANKAR[2,3]

[1]*Department of Information Systems, Statistics & Management Science, The University of Alabama Tuscaloosa, AL 35487, USA*
[2]*Department of Industrial Engineering, University of Pittsburgh, Pittsburgh, PA 15261, USA*
E-mail: jkharouf@pitt.edu.
[3]*Department of Mechanical Engineering and Materials Science, University of Pittsburgh, Pittsburgh, PA 15261, USA*

Received June 2010 and accepted May 2011

Endowing conventional microcrystalline materials with nanometer-scale grains at the surfaces can offer enhanced mechanical properties, including improved wear, fatigue, and friction properties, while simultaneously enabling useful functionalizations with regard to biocompatibility, osseointegration, electrochemical performance, etc. To inherit such multifunctional properties from the surface nanograined state, existing approaches often use coatings that are created through an array of secondary processing techniques (e.g., physical or chemical vapor deposition, surface mechanical attrition treatment, etc.). Obviating the need for such surface processing, recent empirical evidence has demonstrated the introduction of integral surface nanograin structures on bulk materials as a result of severe plastic deformation during machining-based processes. Building on these observations, if empirically driven, process–structure mappings can be developed, it may be possible to engineer enhanced nanoscale surface microstructures directly using machining processes while simultaneously incorporating them within existing computer-numeric-controlled manufacturing systems. Toward this end, this article provides a statistical characterization of nanograined metals created by severe plastic deformation in machining-based processes that maps machining conditions to the resulting microstructure, namely, the mean grain size. A specialized designed experiments approach is used to hypothesize and test a linear mixed-effects model of two important machining parameters. Unlike standard analysis approaches, the statistical dependence between subsets of experimental grain size observations is accounted for and it is shown that ignoring this inherent dependence can yield misleading results for the mean response function. The statistical model is applied to pure copper specimens to identify the factors that most significantly contribute to variability in the mean grain size and is shown to accurately predict the mean grain size under a few scenarios.

Keywords: Nanostructured materials, mean grain size, mixed-effects model

1. Introduction

Manufacturing processes have always sought to endow accurate geometric and topographical attributes while simultaneously controlling performance attributes such as strength, fatigue life, wear behavior, biological response, corrosion resistance, and others. It is well known that controlling the manufacturing process via a science-based understanding of the process–structure–performance triad can significantly expand the product design space and lead to state-of-the-art manufacturing processes that yield products with superior performance properties. Emerging thrusts in nanomanufacturing and nanomaterials have sought to manipulate the organization of crystal structure at nanometer length scales to favorably modulate the property combinations. Nanocrystallinity on surfaces demonstrably enhances mechanical, biological, and corrosion properties as compared to the conventional microcrystalline state (Di Schino *et al.*, 2003; Mishra and Balasubramaniam, 2004; Misra *et al.*, 2009b). As a result, some of the broadest efforts in the area of nanomaterials have focused on creating controlled nanoscale microstructures at the surfaces, often using an array of secondary processing approaches, including chemical and physical deposition techniques, mechanical surface modification, etc. Much of this nanoprocessing often seeks to enhance the underlying microscale crystalline structure that typically results from several conventional metal-forming operations such as rolling, forging, and others, where the process–structure mappings are generally well established.

In contrast to conventional metal forming, an understanding of the evolution of microstructures from machining-based metal cutting processes is complex and

*Corresponding author

still incomplete. However, emerging evidence suggests that peculiarities of the metal cutting process might, in fact, offer opportunities for controlling nanoscale surface grain structures (Calistes *et al.*, 2009) to obviate the need for secondary nanomanufacturing steps aimed at engineering multifunctional properties. To date, manufacturing engineers and scientists have predominantly remained focused on the metrology and modeling of the surface geometry, roughness, mechanics of material removal, and dynamics of the cutting forces, despite the fact that it is known that material removal by metal cutting is a Severe Plastic Deformation (SPD) process that imposes very large strains ($\gg 1$) at high rates (up to 10^5/s) and coupled dynamic temperature rise in the deformation zone. Even a cursory application of the principles of physical metallurgy indicates that such deformation must entail dramatic microstructure transformations involving the accumulation of abnormally high defect densities in the deformation zone. When high defect densities are accumulated, the chip and the machined surface will inherit a severely transformed nanoscale structure that differs dramatically from the bulk material. Nanoscale transformations involving the accumulation, dynamic rearrangement, and recovery of high-density crystal defects under SPD conditions can bequeath an integral nanograined microstructure at the freshly generated surfaces. Such nanograined surface microstructures can play a central role in determining performance attributes such as fatigue life, wear behavior, or corrosion resistance that determine the life cycle of machined components in an array of critical engineering applications. However, despite the prevalence of machining operations in the manufacture of critical components, the manufacturing community does not currently possess a holistic data or knowledge base of the surface microstructures and crystallography inherited by components subsequent to machining operations.

From a technological standpoint, the ability to introduce surface nanograin structures on bulk materials directly through machining-based processes can offer a scalable manufacturing framework for engineering novel surfaces. Currently, approaches for enhancing surface mechanical properties utilize coatings that are created through an array of secondary processing techniques such as physical or chemical vapor deposition or mechanical treatments such as surface mechanical attrition treatment (Roland *et al.*, 2006). If empirically derived process–structure mappings can be developed using the approaches delineated herein, it may be possible to engineer enhanced ultra-fine surface microstructures directly using machining processes while simultaneously incorporating them within existing manufacturing systems. From a materials processing science perspective, these mappings can help elucidate the evolution of grain structure under the simultaneous application of high strains, strain rates, and dynamic temperature, a regime that is currently characterized by remarkably sparse empirical data sets.

It has been recently demonstrated that the SPD during chip formation by machining leads to *both* a nanostructured chip and a nanostructured machined surface, even when the bulk material is a conventional microcrystalline system (Shankar *et al.*, 2005, 2006, 2007; Sevier *et al.*, 2006; Calistes *et al.*, 2009). This discovery has crucial implications for the machining and broader manufacturing communities. It is well known that the nanostructured state involves strength, wear, fretting, fatigue, biological, and electro-chemical properties that are substantially different than those of the conventional microcrystalline state (Valiev *et al.*, 2000; Di Schino *et al.*, 2003; Mishra and Balasubramaniam, 2004; Zhang *et al.*, 2005; Iglesias *et al.*, 2007). Therefore, it is crucial to consider the nanostructural nature of the machined component's surface during the design, manufacture, and life cycle analysis of the product, particularly for applications in which the surface properties and structure are critical. To this end, it is imperative to (i) develop a metrological framework for characterizing the nanostructural nature of machined surfaces and (ii) create process–microstructure mappings that relate surface microstructures to machining parameters. Neither of these frameworks currently exists.

The main objective of this article is to take a first step toward addressing the latter need by developing and analyzing a statistical model of surface microstructure via a designed experiments approach that can be used to map a few machining parameters to the resulting transformed microstructure. The implications of developing such a framework are potentially enormous. If these process–microstructure mappings can be harnessed to custom design surface nanostructures, it will be possible to directly utilize machining-based processes to create refined nanograins on surfaces to exploit the unique phenomena operative at the nanoscale and endow multifunctional property combinations. Furthermore, if the potential for significant technological breakthroughs wrought by recent research on nanostructured/nanocrystalline materials is any indication (Valiev *et al.*, 2000, 2007), the implications of a simple machining-based approach for creating nanograined surfaces can be expected to stimulate innovative product and manufacturing process design opportunities.

Currently, there is a significant gap in empirical data and a gap in what is known about the microstructures resulting from SPD in machining. Addressing the data gap is especially urgent because there have been no comprehensive, quantitative, modern electron microscopic studies of the nanostructures generated by machining operations. However, even if empirical data are made available, a formalized statistical framework for relating microstructural characteristics to the machining parameters has not yet been established. Our aim here is to lay a foundation for addressing the second point. To this end, we present non-standard statistical techniques that can be used to relate common

machining parameters to the resulting refined grain structures from SPD. Although the resulting microstructure can be described by an estimated grain size distribution, our focus here is the characterization of the mean grain size.

The remainder of the article is organized as follows. Section 2 reviews literature pertaining to the analysis of microstructure that is relevant to our work. Section 3 describes the experimental test bed we will use to develop and analyze our statistical model. In Section 4, we formally describe the statistical model for characterizing the microstructure of chips obtained from machining processes (namely the mean grain size). Variants of the general model can be used to account for different model assumptions. Section 5 illustrates the use of the model, describes important analysis pitfalls, and summarizes the results of the statistical experiments. Finally, Section 6 provides some concluding remarks and discusses future potential applications of this work.

2. Relevant literature

Machining processes impart SPD to the chip and the newly formed surface that results in a microstructure that differs significantly from that of the bulk material. Moreover, machining induces large strains at high strain rates along with a dynamic *in situ* temperature rise, which engenders nanograined or ultra-fine grained microstructure in the chip as well as on the freshly machined surface (Shaw, 1984; Shankar *et al.*, 2005, 2006, 2008; Huang *et al.*, 2008; Cai *et al.*, 2009; Calistes *et al.*, 2009). As noted in Section 1, microstructure is the central element that determines the mechanical and other characteristic responses of the material.

Nanostructured materials have been shown to exhibit superior mechanical properties (e.g., increased yield strength up to an order of magnitude higher than their coarse-grained counterparts) and mass transport properties (e.g., enhanced diffusion, which can be several orders of magnitude higher). Some important studies verifying the superior properties of nanostructured surfaces include Horvath (1990), Hofler *et al.* (1993), Youngdahl *et al.* (2001), Valiev *et al.* (2002), and Tao *et al.* (2007). Materials with a nanostructured surface layer have also been shown to be endowed with improved mechanical and other microstructure-dependent multifunctional characteristics like corrosion and electrochemical and biological responses (Hofler *et al.*, 1993; Tao *et al.*, 2003; Roland *et al.*, 2006; Op't Hoog *et al.*, 2008; Shi and Han, 2008; Misra *et al.*, 2009a, 2009b; Raman and Gupta, 2009). For example, it was shown in Tao *et al.* (2003) that nanostructured surfaces of thickness as small as 50 μm can enhance the wear properties in iron, while Roland *et al.* (2006) have shown improved fatigue life for steel with a nanograined layer smaller than 100 μm in thickness. In addition to improved wear properties, improved oxidation resistance and corrosion resistance properties have been demonstrated as a result of finer grain size (Op't Hoog *et al.*, 2008; Raman and Gupta, 2009). Another intriguing characteristic displayed by nanostructured surfaces is their biological responses, such as the enhanced cell–substrate interaction for preosteoblasts on nanostructured and ultra-fine-grained stainless steel (Misra *et al.*, 2009a, 2009b). In those works, the authors demonstrated that materials with nano- and ultra-fine-grained surfaces amplify cell adhesion, viability, and interconnectivity of preosteoblasts in cell cultures as compared to that in coarse-grained surfaces. All of these properties and phenomena are a direct function of the microstructure of the surface that can be quantitatively characterized using two important attributes: the grain size distribution and the distribution of grain and sub-grain misorintations.

Statistical methods have been employed to extract information from microstructures and to determine material properties and the cause-and-effect relationship with initial processing parameters (Torquato, 2002; Al-Ostaz *et al.*, 2007; Grosselle *et al.*, 2010). Some of these works have focused on using statistical methods, like correlation techniques, to reconstruct the complete microstructure in order to determine material properties of disordered materials (Torquato, 2002). While this may be a very useful method, it is very resource intensive and not easy to implement for all conditions. Moreover, it does not establish a direct relation between the initial parameters and the microstructure.

Other researchers have attempted to quantify microstructural information and relate it to material properties (Al-Ostaz *et al.*, 2007; Grosselle *et al.*, 2010). Al-Ostaz *et al.* (2007) have statistically characterized the randomness in morphology in terms of spatial dispersion of inclusions in composites with the aim of classifying microstructural arrangements and relating them to the local stress fields. Grosselle *et al.* (2010) have used traditional Design-Of-Experiment (DOE) techniques and Analysis Of Variance (ANOVA) to determine the significance of factors (e.g., casting speed, copper content, titanium content, heat treatment) on mechanical properties (e.g., yield strength and ductility). While initial processing parameters indeed affect the material properties, these changes in properties are mediated through changes in microstructure, and the complex interplay of the initial conditions can result in unexpected changes in properties that may not be captured directly. For example, in the case of machining, strain and strain rate lead to an *in situ* temperature rise in the material and can result in recovery and recrystallization. Thus, while it is expected that an increase in strain and strain-rate leads to finer grain size (and, hence, higher strength), at very high strain and strain rate, the ensuing temperature rise can result in bimodal grain size distributions that yield appealing property combinations such as high ductility and high yield strength (Shekhar *et al.*, 2009, 2011). These transformations are best captured in terms of microstructural changes, rather than directly relating to property changes, which are an outcome of the complex interplay of these transformations in conjunction with other

parameters. Moreover, once the microstructure can be characterized based on these initial conditions, it can be used to predict various microstructure-dependent characteristics and phenomenon exhibited by the material, and its usefulness will not be limited to any one specific property. Grosselle *et al.* (2010) have also employed standard DOE techniques to relate initial parameters to some of the microstructural features like precipitate size and texture. However, they look into specific properties by simple correlation techniques.

The primary aim of this research is to create a predictive statistical model of ultra-fine-grained structures as a function of important machining parameters, which, in turn, can be used to determine the mechanical and other microstructure-controlled properties. We consider as the main response the grain size that results from a cutting operation. A specialized designed experiments approach is proposed that is capable of handling the non-normality of the grain size distribution and the inherent dependence of grain size observations. This framework can be extended to microstructures created by other processes. Before presenting our statistical model, we first describe the experimental setup and the means by which samples were created and analyzed.

3. Description of experiments

As a test bed for our proposed approach, we considered the process of machining copper bars and subsequently using electron microscopy to statistically examine the resulting microstructure, namely, the distribution of grain sizes. In this study, we examine the grain structure in a chip that has undergone SPD by machining. Prior research has demonstrated that chip formation in machining occurs in a fan-shaped deformation zone ahead of the cutting tool that is the progenitor of similar levels of extreme deformation in both the chip and the freshly created, machined surface (Huang *et al.*, 2008). This has often been shown to result in a nanostructured chip that closely resembles the ultra-fine-grain structure of the machined surface (Calistes *et al.*, 2009). Therefore, it is reasonable to treat the chip as a common archetype of the transformed grain structure resulting from SPD in machining for a given strain and strain rate.

The two primary parameters that determine the final microstructure during machining are strain and deformation rate for a given material system. The initial microstructure of the material (before machining) is also important; however, one can control for initial microstructure by starting with a fully annealed material in each experiment. The configuration of a typical machining process is illustrated in Fig. 1, which depicts the workpiece and the cutting tool. In machining, strain is directly related to the rake angle of the cutting tool, measured away from the normal of the cutting surface (see Fig. 1), and the deformation rate is directly correlated with the relative velocity V between the cutting tool and the workpiece (Shaw, 1984); thus, the final

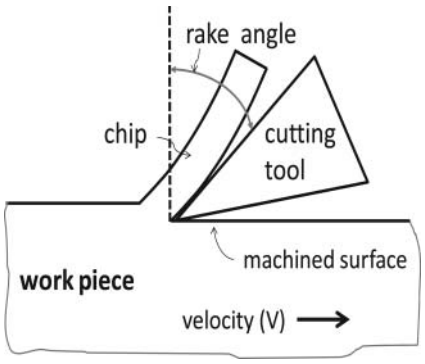

Fig. 1. Configuration of a typical machining process.

microstructure is primarily a function of two machining parameters, the rake angle and V.

For the experiments performed in this research, we used 2-inch-diameter commercially pure copper bars as our starting material and annealed the bars at 700°C for 2 h in order to ensure a fully coarsened initial microstructure. The annealed copper rod was then machined using two different rake angles, 0° and 20°, at two different cutting speeds: low (50 mm/s) and high (1250 mm/s). The deformation parameters were set to ensure a predominantly plane-strain configuration while ensuring that the undeformed chip thickness (0.17 mm) is much smaller than the width of the deformed chip (3 mm; Shaw, 1984). Therefore, the designed experiment considers two factors with two levels each and four treatments labeled as follows: 0L, 0H, 20L, and 20H. Two independent replications of each treatment combination were performed.

All of the different sample conditions were placed in a scanning electron microscope for EBSD-based orientation imaging microscopy (OIM). OIM was carried out using the Phillips XL-30 system equipped with the EDAX-Ametek EBSD detector featuring a Hikari Camera and TSL OIM software for data acquisition and analysis. All scans were taken using a step size of 0.1 μm, and a minimum scan size of 15 μm × 15 μm was used. A 15° grain tolerance was used to obtain an estimated grain size distribution for each scan using the TSL OIM analysis software. At least two scans were completed for each treatment in order to obtain independent replications. Figures 2 and 3 provide grain maps showing the grain size variation under two different processing conditions. In these figures, the different shades depict different grains on the chip.

In Fig. 2, we note that the grain size distribution using the low rake angle and the low cutting speed has a form that differs significantly from that of the case when the rake angle is 20° and the cutting speed is high (see Fig. 3). The probability density estimates were created using kernel density estimators with Gaussian kernel functions (see Silverman (1986)). These figures demonstrate the wide variety of grain size distributions that can be observed, depending on the machining conditions. Ideally, one would

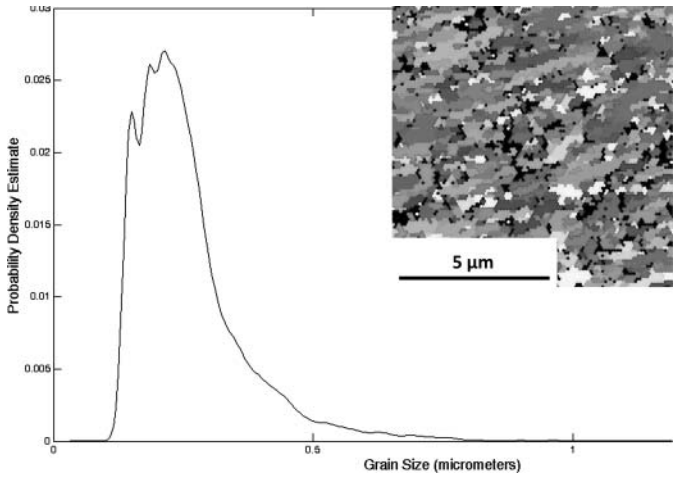

Fig. 2. Estimated grain size distribution (0L). Different shades correspond to different grains.

like to predict the resulting grain size distribution for a fixed set of conditions; however, the lack of empirical data to support a wide range of conditions and/or material systems does not currently exist.

The traditional way to determine the statistical significance of factor effects on a response (e.g., grain size) is to employ standard DOE techniques that examine a few factors at a few levels. Unfortunately, the problem of designing and analyzing experiments of the kind considered in this article is hardly standard due to the hierarchical nature of the experiments. These experiments employ three different randomization procedures in collecting the data, implying that the experiments are not conducted in a completely randomized fashion. The first procedure corresponds to randomly sampling a test specimen (e.g., a copper bar stock) from a larger population of available material. The specimen is then machined with factors set in accordance with the assigned treatment combination (e.g., high rake angle and low cutting speed), resulting in a population of severely deformed machined surface samples (chips). The second randomization procedure randomly selects one (or more) samples from this population for electron microscopy to measure the sizes and misorientation angles of the grains produced by machining. The third randomization procedure randomly selects a subset of grains for observation from the overall population of measured grains. Completely randomized experiments are not feasible since the population of grains is unavailable until after the machining process is complete (i.e., treatments cannot be applied directly to the grains). Therefore, the units of observation (the grains) are nested observations; that is, grains are nested within machined surface samples, and samples are nested within each specimen. Following an experiment conducted at a given treatment combination, several *repeated measures* of grain size are collected for analysis. As a result, observations drawn from a single experimental unit are correlated. This correlation between observations complicates the resulting analysis of the experimental data, relative to standard DOE analysis techniques. In this article, we take a first step toward predicting grain size for a fixed set of processing conditions by introducing a linear mixed-effects model of the mean grain size that accounts for the non-normality of, and correlation between, the grain size observations.

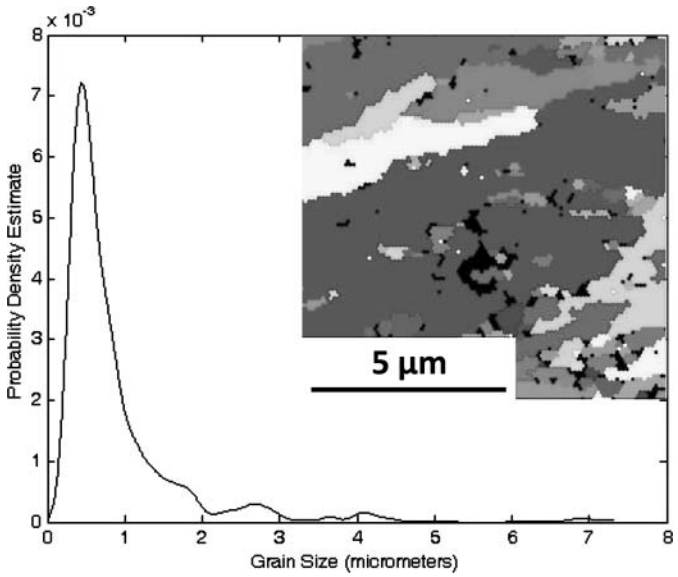

Fig. 3. Estimated grain size distribution (20H). Different shades correspond to different grains.

4. Statistical model description

This section provides our statistical model to describe the machined surface microstructure by examining the response of grain size using a DOE approach. Before we present the model, it is important to note two important issues. First, to employ *standard* DOE techniques, the response observations need to be independent normal random variables. Using grain size as the response, Figs. 2 and 3 demonstrate that the grain size distribution is, in general, non-normal; i.e., the observed grain sizes appear to be highly right-skewed. Moreover, due to the restriction in randomization of the experiments, grain sizes measured from the same microscopy scan are generally correlated. Second, the designed experiments considered in this article are complicated because each scan results in a (random) number of grain size observations; i.e., the experiment is a repeated measures experiment wherein the number of observations taken at each experimental design point is random. This significantly complicates the analysis of these data and suggests the need for a transformation of the data and specialized techniques for identifying and analyzing the main contributors to variance in the resulting microstructure.

We pause here to state a few important assumptions before presenting a general statistical model that can be tailored to our problem.

A1: The samples have identical initial microstructure (before machining).
A2: Exactly one chip is sampled for scanning in the electron microscope, and all chips are representative of the true microstructure.
A3: There are no statistical differences between different bar stock samples originating from the same producer.

In what follows, we introduce a generic model that allows for relaxation of the above assumptions. As we shall see, the model simplifies as these assumptions are imposed.

The primary response of interest is the grain size that results in the chip (and machined surface) after machining. For the response of grain size, we propose a linear statistical model of the form

$$y_{ijk} = \mathbf{z}_i^{'}\boldsymbol{\beta} + \delta_i + \nu_{ij} + \epsilon_{ijk}, \tag{1}$$

where y_{ijk} denotes the kth grain size sampled from the jth chip of bar stock i for $i = 1, \ldots, N$, $j = 1, \ldots, m_i$ and $k = 1, \ldots, n_{ij}$, where N denotes the number of bars used in the experiment, m_i is the number of chips sampled from bar stock i, and n_{ij} denotes the number of grain sizes sampled from the jth chip of bar stock i. Let p denote the number of fixed effects in the model (including an intercept term). The remaining model parameters are defined as follows:

$\mathbf{z}_i$: a $p \times 1$ vector corresponding to the treatment combination applied to bar stock i;
$\boldsymbol{\beta}$: a $p \times 1$ vector of unknown fixed effects;
$\delta_i \sim N(0, \sigma_\delta^2)$: a random component due to sampling bar stock i;
$\nu_{ij} \sim N(0, \sigma_\nu^2)$: a random component due to sampling chip j from bar stock i;
$\epsilon_{ijk} \sim N(0, \sigma_\epsilon^2)$: a random component due to sampling kth grain on jth chip of bar stock i,

where $N(0, x^2)$ denotes a zero-mean normal random variable with variance x^2. The model assumes that δ_i, ν_{ij}, and ϵ_{ijk} are mutually independent for all i, j, k. Therefore,

$$E(y_{ijk}) = \mathbf{z}_i^{'}\boldsymbol{\beta},$$

for each i, j, k, and the covariance structure for the observations y_{ijk} is given by

$$\mathrm{Cov}(y_{ijk}, y_{i'j'k'}) = \begin{cases} \sigma_\delta^2 + \sigma_\nu^2 + \sigma_\epsilon^2, & i = i',\ j = j',\ k = k', \\ \sigma_\delta^2 + \sigma_\nu^2, & i = i',\ j = j',\ k \neq k', \\ \sigma_\delta^2, & i = i',\ j \neq j', \\ 0, & i \neq i'. \end{cases}$$

Let $\mathbf{y}_i = [\mathbf{y}_{i1}', \mathbf{y}_{i2}', \ldots, \mathbf{y}_{im_i}']'$, where $\mathbf{A}'$ denotes the transpose of the matrix $\mathbf{A}$:

$$\mathbf{y}_{ij} = \mathbf{1}_{n_{ij}}\mathbf{z}_i^{'}\boldsymbol{\beta} + \mathbf{1}_{n_{ij}}\delta_i + \mathbf{1}_{n_{ij}}\nu_{ij} + \boldsymbol{\epsilon}_{ij},$$

denotes the vector of observations taken from the jth chip of bar stock i, and $\mathbf{1}_{n_{ij}}$ is an $n_{ij} \times 1$ vector of ones. Then

$$E(\mathbf{y}_i) = \boldsymbol{\mu}_i = \mathbf{1}_{n_{i\cdot}}\mathbf{z}_i^{'}\beta,$$

where $n_{i\cdot} = \sum_{j=1}^{m_i} n_{ij}$, and

$$\mathrm{Var}(\mathbf{y}_i) = \mathbf{V}_i = \begin{bmatrix} \mathbf{V}_{i1} & \sigma_\delta^2\mathbf{1}_{n_{i1}}\mathbf{1}_{n_{i2}}^{'} & \cdots & \sigma_\delta^2\mathbf{1}_{n_{i1}}\mathbf{1}_{n_{im_i}}^{'} \\ \sigma_\delta^2\mathbf{1}_{n_{i2}}\mathbf{1}_{n_{i1}}^{'} & \mathbf{V}_{i2} & \cdots & \sigma_\delta^2\mathbf{1}_{n_{i2}}\mathbf{1}_{n_{im_i}}^{'} \\ \vdots & \vdots & \ddots & \vdots \\ \sigma_\delta^2\mathbf{1}_{n_{im_i}}\mathbf{1}_{n_{i1}}^{'} & \sigma_\delta^2\mathbf{1}_{n_{im_i}}\mathbf{1}_{n_{i2}}^{'} & \cdots & \mathbf{V}_{im_i} \end{bmatrix}, \tag{2}$$

whose diagonal elements are given by

$$\mathbf{V}_{ij} = \sigma_\delta^2\mathbf{1}_{n_{ij}}\mathbf{1}_{n_{ij}}^{'} + \sigma_\nu^2\mathbf{1}_{n_{ij}}\mathbf{1}_{n_{ij}}^{'} + \sigma_\epsilon^2\mathbf{I}_{n_{ij}}.$$

For convenience, let $\phi \equiv [\sigma_\delta^2,\ \sigma_\nu^2,\ \sigma_\epsilon^2]$ be the vector of variance components.

If we impose Assumption A2 that only a single chip is sampled from each bar (i.e., $m_i = 1$ for all i), then

$$\mathbf{V}_i = \mathbf{V}_{i1} = \sigma_b^2\mathbf{1}_{n_{i1}}\mathbf{1}_{n_{i1}}^{'} + \sigma_\epsilon^2\mathbf{I}_{n_{i1}}, \tag{3}$$

where $\sigma_b^2 = \sigma_\delta^2 + \sigma_\nu^2$ denotes a confounded measure of variability due to bar stock *and* chip. The term *confounded* implies that although we can estimate σ_b^2, we cannot distinguish between σ_δ^2 and σ_ν^2.

Suppose we assume that $\sigma_\delta^2 = 0$; i.e., there is no *random* effect due to bar stock as stipulated by Assumption A3. Then, the variance–covariance matrix of $\mathbf{y}_i$ in Equation (2) takes the form:

$$\mathbf{V}_i = \begin{bmatrix} \mathbf{V}_{i1} & \mathbf{0} & \cdots & \mathbf{0} \\ \mathbf{0} & \mathbf{V}_{i2} & \cdots & \mathbf{0} \\ \vdots & \vdots & \ddots & \vdots \\ \mathbf{0} & \mathbf{0} & \cdots & \mathbf{V}_{im_i} \end{bmatrix} \tag{4}$$

where

$$\mathbf{V}_{ij} = \sigma_\nu^2\mathbf{1}_{n_{ij}}\mathbf{1}_{n_{ij}}^{'} + \sigma_\epsilon^2\mathbf{I}_{n_{ij}}.$$

Note that Equation (2) suggests that if $\sigma_\delta^2 = 0$, then chips sampled from the ith bar stock are *true replicates*. On the other hand, if $\sigma_\delta^2 > 0$, then chips sampled from the ith bar stock are *repeated measures*. The next subsection is focused on estimating the unknown parameter vectors $\boldsymbol{\beta}$ and $\boldsymbol{\phi}$.

4.1. *Model estimation*

In this subsection we discuss two methods for estimating the unknown parameters $\boldsymbol{\beta}$ and $\boldsymbol{\phi}$ of Model (1). The first approach involves maximization of the full likelihood of the response data, whereas the second approach involves the maximization of a partial likelihood. The latter approach, Restricted Maximum Likelihood (REML), is often

preferred over the former due to its effectiveness in eliminating the bias in the variance component estimates as a result of estimating the fixed-effects component of the model. However, arguments such as those given in Harville (1977) suggest that there may not be a clear "winner" between the two methods. Therefore, we present both methods for completeness. The following developments are for the case where $\sigma_\delta^2 = 0$, as stipulated by Assumption A3.

4.1.1. *Method of maximum likelihood*

The Maximum Likelihood (ML) approach to parameter estimation in the general linear mixed-effects model was first developed by Hartley and Rao (1967). To apply their approach to our experiments, let $\mathbf{y} = [\mathbf{y}_1', \mathbf{y}_2', \ldots, \mathbf{y}_N']'$ denote the $a \times 1$ observed response vector for the experiment, where $a = \sum_i \sum_j n_{ij} = \sum_i n_{i\cdot}$ denotes the total number of observations. Then, under multivariate normal model assumptions, the log-likelihood function of β and ϕ is given by

$$\ell(\phi, \beta|\mathbf{y}) = -\sum_{i=1}^{N}\sum_{j=1}^{m_i} \ln|\mathbf{V}_{ij}| - \sum_{i=1}^{N}\sum_{j=1}^{m_i}(\mathbf{y}_{ij} - \mathbf{1}_{n_{ij}}\mathbf{z}_i'\beta)'\mathbf{V}_{ij}^{-1} \times (\mathbf{y}_{ij} - \mathbf{1}_{n_{ij}}\mathbf{z}_i'\beta), \quad (5)$$

where $\ln = \log_e$ and $\mathbf{V}_{ij}$ denotes the variance–covariance matrix corresponding to the observations obtained from the jth chip of bar stock i. In what follows, note that $\mathbf{V}_{ij}$ can be written as

$$\mathbf{V}_{ij} = \phi_1\mathbf{V}_{ij1} + \phi_2\mathbf{V}_{ij2}, \quad (6)$$

where $\mathbf{V}_{ij1} = \mathbf{1}_{n_{ij}}\mathbf{1}_{n_{ij}}'$, $\mathbf{V}_{ij2} = \mathbf{I}_{n_{ij}}$, and ϕ_1 and ϕ_2 are unknown parameters. To derive the stationary equations, we first differentiate the log-likelihood function (5) with respect to the unknown parameters ϕ_r to obtain

$$\frac{\partial\ell(\boldsymbol{\phi}, \boldsymbol{\beta}|\mathbf{y})}{\partial\phi_r} = -\sum_{i=1}^{N}\sum_{j=1}^{m_i}\mathrm{tr}\left(\mathbf{V}_{ij}^{-1}\mathbf{V}_{ijr}\right) + \sum_{i=1}^{N}\sum_{j=1}^{m_i}\rho_{ijr}, \quad r = 1, 2,$$

where $\mathrm{tr}(\mathbf{A})$ denotes the trace of matrix $\mathbf{A}$ and

$$\rho_{ijr} = (\mathbf{y}_{ij} - \mathbf{1}_{n_{ij}}\mathbf{z}_i'\boldsymbol{\beta})'\mathbf{V}_{ij}^{-1}\mathbf{V}_{ijr}\mathbf{V}_{ij}^{-1}(\mathbf{y}_{ij} - \mathbf{1}_{n_{ij}}\mathbf{z}_i'\boldsymbol{\beta}).$$

Note that we can write:

$$\mathrm{tr}\left(\mathbf{V}_{ij}^{-1}\mathbf{V}_{ijr}\right) = \phi_1\omega_{ijr1} + \phi_2\omega_{ijr2},$$

where

$$\omega_{ijrs} = \mathrm{tr}\left(\mathbf{V}_{ij}^{-1}\mathbf{V}_{ijr}\mathbf{V}_{ij}^{-1}\mathbf{V}_{ijs}\right),$$

for $s = 1, 2$. Therefore, if we define the 2×2 matrices $\boldsymbol{\Omega}_{ij} = \{\omega_{ijrs}\}$, then the stationary equations for any given $\boldsymbol{\beta}$ are

$$\sum_{i=1}^{N}\sum_{j=1}^{m_i}\boldsymbol{\Omega}_{ij}\boldsymbol{\phi} = \sum_{i=1}^{N}\sum_{j=1}^{m_i}\boldsymbol{\rho}_{ij},$$

where

$$\boldsymbol{\rho}_{ij} = \begin{bmatrix} (\mathbf{y}_{ij} - \mathbf{1}_{n_{ij}}\mathbf{z}_i'\boldsymbol{\beta})'\mathbf{V}_{ij}^{-1}\mathbf{1}_{n_{ij}}\mathbf{1}_{n_{ij}}'\mathbf{V}_{ij}^{-1}(\mathbf{y}_{ij} - \mathbf{1}_{n_{ij}}\mathbf{z}_i'\boldsymbol{\beta}) \\ (\mathbf{y}_{ij} - \mathbf{1}_{n_{ij}}\mathbf{z}_i'\boldsymbol{\beta})'\mathbf{V}_{ij}^{-1}\mathbf{V}_{ij}^{-1}(\mathbf{y}_{ij} - \mathbf{1}_{n_{ij}}\mathbf{z}_i'\boldsymbol{\beta}) \end{bmatrix},$$

and thus the estimate of $\boldsymbol{\phi}$ is obtained iteratively by

$$\tilde{\boldsymbol{\phi}}(\boldsymbol{\beta}) = \left(\sum_{i=1}^{N}\sum_{j=1}^{m_i}\boldsymbol{\Omega}_{ij}\right)^{-1}\left(\sum_{i=1}^{N}\sum_{j=1}^{m_i}\rho_{ij}\right).$$

The stationary equations with respect to $\boldsymbol{\beta}$ are easily shown to be

$$\left[\sum_{i=1}^{N}\sum_{j=1}^{m_i}(\mathbf{z}_i\mathbf{1}_{n_{ij}}'\mathbf{V}_{ij}^{-1}\mathbf{1}_{n_{ij}}\mathbf{z}_i')\right]\beta = \sum_{i=1}^{N}\sum_{j=1}^{m_i}\mathbf{z}_i\mathbf{1}_{n_{ij}}\mathbf{V}_{ij}^{-1}\mathbf{y}_{ij},$$

so that

$$\tilde{\beta}(\phi) = \left[\sum_{i=1}^{N}\sum_{j=1}^{m_i}(\mathbf{z}_i\mathbf{1}_{n_{ij}}'\mathbf{V}_{ij}^{-1}\mathbf{1}_{n_{ij}}\mathbf{z}_i')\right]^{-1}\left[\sum_{i=1}^{N}\sum_{j=1}^{m_i}\mathbf{z}_i\mathbf{1}_{n_{ij}}'\mathbf{V}_{ij}^{-1}\mathbf{y}_{ij}\right].$$

This estimation procedure relies on the assumption that the $\mathbf{y}_i$ values are mutually independent and multivariate normal with mean vector $\boldsymbol{\mu}_i$ and variance–covariance matrix $\mathbf{V}_i$. Unfortunately, the grain size distributions tend to be highly right-skewed (see Figs. 2 and 3) and thus are not well approximated by the normal distribution. However, suppose there exists a transformation on $\mathbf{y}_i$ such that the transformed data, say $\mathbf{y}_i(\theta)$, follow the prescribed multivariate normal distribution. For our purposes in this research, we follow Box and Cox (1964) and consider the class of power transformations:

$$y_{ijk}(\theta) = \begin{cases} (y_{ijk}^{\theta} - 1)/\theta, & \theta \neq 0, \\ \ln(y_{ijk}), & \theta = 0, \end{cases} \quad (7)$$

for $i = 1, \ldots, N$, $j = 1, \ldots, m_i$, and $k = 1, \ldots, n_{ij}$, where θ denotes the transformation parameter. The Jacobian determinant of the transformation in Equation (7) is

$$J = \prod_{i=1}^{N}\prod_{j=1}^{m_i}\prod_{k=1}^{n_{ij}} y_{ijk}^{\theta-1},$$

and since the $\mathbf{y}_i(\theta)$ values are assumed to be mutually independent, each following a multivariate normal distribution, the log-likelihood function of the *untransformed* data is then given by

$$\ell(\boldsymbol{\beta}, \boldsymbol{\phi}, \theta) = (\theta - 1)\sum_{i=1}^{N}\sum_{j=1}^{m_i}\sum_{k=1}^{n_{ij}}\ln(y_{ijk}) - \frac{1}{2}\sum_{i=1}^{N}\sum_{j=1}^{m_i}\ln(|\mathbf{V}_{ij}|) - \sum_{i=1}^{N}\sum_{j=1}^{m_i}(\mathbf{y}_{ij}(\theta) - \mathbf{1}_{n_{ij}}\mathbf{z}_i'\boldsymbol{\beta})'\mathbf{V}_{ij}^{-1}(\mathbf{y}_{ij}(\theta) - \mathbf{1}_{n_{ij}}\mathbf{z}_i'\boldsymbol{\beta}). \quad (8)$$

Our objective is to obtain the values of θ, $\boldsymbol{\beta}$, and $\boldsymbol{\phi}$ that maximize $\ell(\boldsymbol{\beta}, \boldsymbol{\phi}, \theta)$.

Note that for a given value of the transformation parameter θ, optimal (or near optimal) values of $\boldsymbol{\beta}$ and $\boldsymbol{\phi}$ can be obtained iteratively by performing the following steps which, as noted by Hocking (2003), are closely related to second-order gradient methods:

Step 1. Choose a value for θ and an initial vector for ϕ, say $\tilde{\phi}^{(0)}$;

Step 2. Compute

$$\mathbf{V}_{ij}^{(0)} = \tilde{\phi}_1^{(0)} \mathbf{1}_{n_{ij}} \mathbf{1}_{n_{ij}}^{'} + \tilde{\phi}_2^{(0)} \mathbf{I}_{n_{ij}}$$

for $i = 1, \ldots, N$ and $j = 1, \ldots, m_i$, and

$$\tilde{\boldsymbol{\beta}}^{(0)}(\theta) = \left[\sum_{i=1}^{N} \sum_{j=1}^{m_i} \left(\mathbf{z}_i \mathbf{1}_{n_{ij}}^{'} \left(\mathbf{V}_{ij}^{(0)} \right)^{-1} \mathbf{1}_{n_{ij}} \mathbf{z}_i^{'} \right) \right]^{-1} \times \left[\sum_{i=1}^{N} \sum_{j=1}^{m_i} \mathbf{z}_i \mathbf{1}_{n_{ij}}^{'} \left(\mathbf{V}_{ij}^{(0)} \right)^{-1} \mathbf{y}_{ij}(\theta) \right];.$$

Step 3. Use $\mathbf{V}_{ij}^{(0)}$'s and $\tilde{\boldsymbol{\beta}}^{(0)}(\theta)$ to evaluate $\boldsymbol{\Omega}_{ij}$ and $\rho_{ij}(\theta)$ (for $i = 1, \ldots, N$ and $j = 1, \ldots, m_i$), then compute

$$\tilde{\boldsymbol{\phi}}^{(1)} = \left(\sum_{i=1}^{N} \sum_{j=1}^{m_i} \boldsymbol{\Omega}_{ij} \right)^{-1} \left(\sum_{i=1}^{N} \sum_{j=1}^{m_i} \rho_{ij}(\theta) \right);$$

Step 4. Return to Step 2 and iterate until $\| \hat{\boldsymbol{\phi}}^{(c)} - \hat{\boldsymbol{\phi}}^{(c-1)} \| < \vartheta$, where c is the iteration index and ϑ ($\vartheta > 0$) is the convergence threshold.

These steps can be performed for a range of θ values, each time substituting the resulting estimates of $\boldsymbol{\beta}$ and $\boldsymbol{\phi}$ in Equation (8) and retaining that value of θ that maximizes $\ell(\boldsymbol{\beta}, \boldsymbol{\phi}, \theta)$. We suggest using values of θ in the set $[-1, 1]$ in increments of 0.5. These values include a number of important transformations such as the inverse, inverse square-root, natural logarithm, and square-root transformations, as well as the untransformed case ($\theta = 1$). Values of θ outside of this range can be more difficult to interpret in practice. For each of the experiments that follow in Section 5, we chose the convergence threshold $\vartheta = 0.000\,001$.

4.1.2. *REML*

The ML method outlined provides (asymptotically) consistent estimators of the variance components (see Hartley and Rao (1967)). However, for finite samples, it is well known that the ML approach produces estimates of the variance components that are biased downwards (c.f. Patterson and Thompson (1971) and Corbeil and Searle (1976)). This bias stems from the loss in degrees of freedom as a result of estimating the fixed effects in the model. To illustrate this bias, consider a finite sample, $X_1, X_2, \ldots, X_N$, drawn randomly from a normal population. If these observations are independent and identically distributed with unknown mean μ and variance σ_X^2, then the maximum likelihood estimator for σ_X^2 is

$$S_X^2 = \frac{1}{N} \sum_{i=1}^{N} (X_i - \bar{X})^2, \tag{9}$$

where $\bar{X} = (1/N) \sum_{i=1}^{N} X_i$. Applying the expectation operator to Equation (9) we see that:

$$E\left(S_X^2\right) = \left(\frac{N-1}{N} \right) \sigma_X^2 < \sigma_X^2,$$

showing that S_X^2 is biased downward. This bias is a direct result of not accounting for the single degree of freedom loss due to estimating the population mean μ.

In order to remove the bias in the ML estimates of the variance components, we employ REML as proposed by Corbeil and Searle (1976). The theoretical underpinnings of the method involve a factorization of the full log-likelihood function of Equation (5) into two parts, one depending only on $\boldsymbol{\phi}$. The maximizer of this "partial" likelihood function is then used to estimate the variance components. Details of the factorization are described in Corbiel and Searle (1976), Harville (1977), and Hocking (2003).

To incorporate the class of power transformations defined in Equation (7) for the REML case, we take an approach similar to that described by Gurka *et al.* (2006). We seek values of ϕ_1, ϕ_2, and θ that maximize the following *restricted* log-likelihood of the *untransformed* data:

$$\begin{aligned} \ell_{\mathrm{R}}(\boldsymbol{\phi}, \theta) = (\theta - 1) & \sum_{i=1}^{N} \sum_{j=1}^{m_i} \sum_{k=1}^{n_{ij}} \ln(y_{ijk}) \\ & - \ln \left| \sum_{i=1}^{N} \sum_{j=1}^{m_i} \mathbf{z}_i \mathbf{1}_{ij}^{'} \mathbf{V}_{ij}^{-1} \mathbf{1}_{ij} \mathbf{z}_i^{'} \right| - \sum_{i=1}^{N} \sum_{j=1}^{m_i} \ln |\mathbf{V}_{ij}| \\ & - \sum_{i=1}^{N} \sum_{j=1}^{m_i} (\mathbf{y}_{ij}(\theta) - \mathbf{1}_{n_{ij}} \mathbf{z}_i^{'} \hat{\boldsymbol{\beta}})' \mathbf{V}_{ij}^{-1} (\mathbf{y}_{ij}(\theta) - \mathbf{1}_{n_{ij}} \mathbf{z}_i^{'} \hat{\boldsymbol{\beta}}) \end{aligned} \tag{10}$$

where $\mathbf{y}_{ij}(\theta)$ denotes the transformed $n_{ij} \times 1$ observation vector obtained from the jth chip of bar stock i, and

$$\hat{\boldsymbol{\beta}} = \hat{\boldsymbol{\beta}}(\boldsymbol{\phi}) = \left[\sum_{i=1}^{N} \sum_{j=1}^{m_i} \left(\mathbf{z}_i \mathbf{1}_{n_{ij}}^{'} \mathbf{V}_{ij}^{-1} \mathbf{1}_{n_{ij}} \mathbf{z}_i \right) \right]^{-1} \times \left[\sum_{i=1}^{N} \sum_{j=1}^{m_i} \mathbf{z}_i \mathbf{1}_{n_{ij}}^{'} \mathbf{V}_{ij}^{-1} \mathbf{y}_{ij} \right].$$

Obtaining REML estimates of the variance components for any given value of θ can be accomplished in a way similar to the ML approach outlined above. Let $\mathbf{W}_{ij} =$

$\mathbf{1}_{n_{ij}}\mathbf{z}_i'$ and define the stacked design matrix $\mathbf{W}$ by

$$\mathbf{W} = [\mathbf{W}_{11}', \mathbf{W}_{12}', \ldots, \mathbf{W}_{1m_1}', \ldots, \mathbf{W}_{N1}', \mathbf{W}_{N2}', \ldots, \mathbf{W}_{Nm_N}']', \tag{11}$$

with dimensions $a \times p$, where a and p were defined previously. Furthermore, define the $a \times a$ block diagonal matrices

$$\mathbf{V} = \begin{bmatrix} \mathbf{V}_{11} & \mathbf{0} & \cdots & \mathbf{0} \\ \mathbf{0} & \mathbf{V}_{12} & \cdots & \mathbf{0} \\ \vdots & \vdots & \ddots & \vdots \\ \mathbf{0} & \mathbf{0} & \cdots & \mathbf{V}_{Nm_N} \end{bmatrix}, \tag{12}$$

$$\tilde{\mathbf{V}}_1 = \begin{bmatrix} \mathbf{V}_{111} & \mathbf{0} & \cdots & \mathbf{0} \\ \mathbf{0} & \mathbf{V}_{121} & \cdots & \mathbf{0} \\ \vdots & \vdots & \ddots & \vdots \\ \mathbf{0} & \mathbf{0} & \cdots & \mathbf{V}_{Nm_N1} \end{bmatrix},$$

and

$$\tilde{\mathbf{V}}_2 = \begin{bmatrix} \mathbf{V}_{112} & \mathbf{0} & \cdots & \mathbf{0} \\ \mathbf{0} & \mathbf{V}_{122} & \cdots & \mathbf{0} \\ \vdots & \vdots & \ddots & \vdots \\ \mathbf{0} & \mathbf{0} & \cdots & \mathbf{V}_{Nm_N2} \end{bmatrix},$$

where, for each i, j, $\mathbf{V}_{ij}$, $\mathbf{V}_{ij1}$, and $\mathbf{V}_{ij2}$ are defined as in Equation (6). Finally, define the stacked $a \times 1$ transformed observation vector $\mathbf{y}(\theta)$ as

$$\mathbf{y}(\theta) = [\mathbf{y}_{11}'(\theta), \mathbf{y}_{12}'(\theta), \ldots, \mathbf{y}_{Nm_N}'(\theta)]'. \tag{13}$$

For a given value of the transformation parameter θ, the methods developed in the last subsection for the ML case can be applied to maximize the REML log-likelihood function, which under the new parameterization can be written as

$$\begin{aligned} \ell_R(\phi, \theta) = (\theta - 1) \sum_{i=1}^{N} \sum_{j=1}^{m_i} \sum_{k=1}^{n_{ij}} \ln(y_{ijk}) \\ - \sum_{i=1}^{N} \sum_{j=1}^{m_i} \ln |\mathbf{V}_{ij}| - \ln |\mathbf{W}'\mathbf{V}^{-1}\mathbf{W}| \\ - (\mathbf{y}(\theta) - \mathbf{W}\hat{\beta})'\mathbf{V}^{-1}(\mathbf{y}(\theta) - \mathbf{W}\hat{\beta}) \end{aligned} \tag{14}$$

where

$$\hat{\beta} = (\mathbf{W}'\mathbf{V}^{-1}\mathbf{W})^{-1}\mathbf{W}'\mathbf{V}^{-1}\mathbf{y}(\theta). \tag{15}$$

It can be shown that the REML stationary equations for $\boldsymbol{\phi}$ are given by

$$\boldsymbol{\Omega}^* \phi = \boldsymbol{\rho}^*(\theta)$$

where $\boldsymbol{\Omega}^*$ is the 2×2 matrix with elements:

$$\omega_{rs}^* = \mathrm{tr}(\mathbf{V}^{-1}\mathbf{M}\tilde{\mathbf{V}}_r\mathbf{M}'\mathbf{V}^{-1}\tilde{\mathbf{V}}_s)$$

$(r, s \in \{1, 2\})$ and $\boldsymbol{\rho}^*(\theta)$ is the 2×1 vector with elements:

$$\rho_r^*(\theta) = \mathbf{y}(\theta)'\mathbf{V}^{-1}\mathbf{M}\tilde{\mathbf{V}}_r\mathbf{M}'\mathbf{V}^{-1}\mathbf{y}(\theta),$$

where

$$\mathbf{M} = \mathbf{I}_a - \mathbf{W}(\mathbf{W}'\mathbf{V}^{-1}\mathbf{W})^{-1}\mathbf{W}'\mathbf{V}^{-1}. \tag{16}$$

As a result, for a given value of θ, REML estimates for ϕ are obtained iteratively from:

$$\tilde{\boldsymbol{\phi}} = (\boldsymbol{\Omega}^*)^{-1}\, \boldsymbol{\rho}^*(\theta),$$

and the estimate for the fixed effects component $\boldsymbol{\beta}$ is then given by (15), where $\mathbf{V}$ is evaluated using the REML estimate for $\boldsymbol{\phi}$.

Note that for a given value of the transformation parameter θ, the value of ϕ that maximizes the restricted log-likelihood function of Equation (10) can be obtained iteratively by performing the following steps:

Step 1. Choose a value for θ and an initial vector for ϕ, say $\tilde{\phi}^{(0)}$;

Step 2. Use $\tilde{\phi}^{(0)}$ to compute $\mathbf{V}^{(0)}$ and $\mathbf{M}^{(0)}$ using Equations (12) and (16), respectively.

Step 3. Use $\mathbf{V}^{(0)}$ and $\mathbf{M}^{(0)}$ to evaluate $\boldsymbol{\Omega}^*$ and $\boldsymbol{\rho}^*(\theta)$, then compute

$$\tilde{\boldsymbol{\phi}}^{(1)} = (\boldsymbol{\Omega}^*)^{-1}\, \boldsymbol{\rho}^*(\theta);$$

Step 4. Return to Step 2 and iterate until $\|\tilde{\phi}^{(c)} - \tilde{\phi}^{(c-1)}\| < \vartheta$.

The REML estimate for $\boldsymbol{\phi}$ obtained from the last iteration, say $\tilde{\boldsymbol{\phi}}$, is substituted into Equation (15) to obtain $\hat{\beta}$. In the next section, we discuss the means by which to draw statistical inference on the fixed-effects parameters of the grain size model given by Equation (1).

4.2. *Model inference*

In this section, we discuss the approach to drawing statistical inference on the fixed-effects component of the model in Equation (1). Suppose that, for some fixed effect h, we are interested in testing the hypothesis:

$$H_0 : \beta_h = 0,$$
$$H_1 : \beta_h \neq 0.$$

A lack of evidence that $\beta_h \neq 0$ suggests that the factor corresponding to β_h is not a significant source of variability in the mean grain size. As a result, one can subsequently preclude the variable from any further analysis.

Asymptotic theory is typically used to develop statistical tests for the fixed-effects component of the model. If the variance components are known, it can easily be shown that:

$$\mathrm{Var}(\hat{\beta}) \equiv \mathbf{D} = \left[\sum_{i=1}^{N} \sum_{j=1}^{m_i} \left(\mathbf{z}_i \mathbf{1}_{n_{ij}}' \mathbf{V}_{ij}^{-1} \mathbf{1}_{n_{ij}} \mathbf{z}_i' \right) \right]^{-1}, \tag{17}$$

and by substituting estimates of the variance components (i.e., $\hat{\phi}$) into $\mathbf{V}_{ij}$, we have the following test statistic:

$$Z_0 = \frac{\hat{\beta}_h}{\sqrt{\hat{D}_{hh}}} \tag{18}$$

which converges in distribution to the standard normal distribution under H_0 as the number of design replicates approaches infinity. Thus, for a given level of significance α (the Type-I error probability), an *approximate* test (due to a finite sample size) involves computing $|Z_0|$ and comparing its value to the upper $\alpha/2$ quantile of the standard normal distribution.

The test described here is reasonable when the experimenter has a large number of design replicates; however, the experiments used to obtain grain size observations via electron microscopy are very expensive and time consuming. Therefore, it is unlikely that a large number of replicates per treatment combination will be available. Consequently, Z_0, although still approximately normal with zero mean under H_0, will have a variance that exceeds unity. Hence, the probability of a false alarm is inflated. That is, the test will more often than expected detect an effect that does not exist.

Rather than relying on asymptotic theory for the percentiles of the null distribution of Z_0, one can rely on the small sample approximations to the null distribution suggested by Satterthwaite (1941) and Kenward and Roger (1997). However, a simpler alternative is to simulate a large number of samples of Z_0 under H_0, given information regarding the amount of replication (which is known), and use these "pseudo-samples" to better approximate the percentiles of the null distribution. This is a feasible approach since the expression in Equation (18) is solely a function of the data. Moreover, ML or REML estimates of σ_v^2 and σ_ϵ^2 can be used when generating the pseudo-samples from the null distribution, and if an orthogonal design is used to collect the data, the null distribution of Equation (18) will be independent of the other effect estimates (i.e., the $\hat{\beta}_{h'}$ values where $h' \neq h$). Consequently, critical values against which to compare the test statistic can be better approximated, thereby reducing the probability of a false alarm. We demonstrate this approach to approximating the null distribution in Section 5 where the experimental analysis results are presented.

It is important to note that if standard DOE methods are used to analyze the problem described here (i.e., a problem with a nested error structure), the effects of treatments applied at the bar stock level may appear to be statistically significant when, in fact, they are not. This is due to the fact that a loss of precision in the estimation of $\boldsymbol{\beta}$ is incurred as a result of sampling less frequently at the bar-stock level relative to the level of chips or grains. When standard DOE methods are used, the estimated standard errors of the resulting $\hat{\boldsymbol{\beta}}$ values will be underestimated in this case, and the magnitude of Z_0 in Equation (18) will more often than not be falsely inflated. This result has been well documented by several authors (see, for example, Kempthorne (1952), Nelson (1985), and Box and Jones (1992)) and is demonstrated in Section 5, which presents the results of our analysis.

5. Experimental results

In this section, we implement and validate the model of Equation (1) to predict mean grain size as a result of two primary factors. Recall that the goal of the experiments is to characterize the variability in the mean grain size (y) as a function of rake angle (factor A) and cutting speed (factor B), as well as their interaction (factor AB). For analysis purposes, it is reasonable to assume that, due to the purity standards of the experimental material, there is no random effect due to bar stock. Thus, we postulate the following model:

$$y_{ijk} = \beta_0 + \beta_1 A + \beta_2 B + \beta_{12} AB + v_{ij} + \epsilon_{ijk}, \tag{19}$$

where β_0, β_1, β_2, and β_{12} denote the fixed-effect components, and v_{ij} and ϵ_{ijk} denote the random components.

An efficient experimental design used to fit the model of Equation (19) is a two-level, full-factorial design (see Montgomery (2009)). In such a design, all possible treatment combinations of q factors (each at two levels) are performed for a total of 2^q experiments. For our problem, $q = 2$ experimental factors, resulting in a 2^2 factorial design. A single replicate of the 2^2 design is shown in Table 1, with A and B in coded form (i.e., -1 and $+1$ for low and high factor levels, respectively). For example, the first row in Table 1 represents the experimental run performed with A and B both at their low levels, the second row represents the experimental run performed with A at its high level and B at its low level, and so forth.

For the experiments analyzed herein, we have at our disposal two replicates of the design in Table 1. Thus, a total of $N = 8$ experiments were performed. For each experiment, we randomly selected a single chip for microscopy scan (i.e., $m_i = 1$ for all i). Also, for each chip selected, we sampled 250 grain sizes, thus, $n_{i1} = 250$ for all i. Therefore, the total number of observations in the experiment is $8 \times 250 = 2000$. It should be noted that the analysis methods discussed in Section 4 do not impose the requirement $n_{ij} = n$ for all i, j. However, since a microscopy scan of any given chip can produce well in excess of 1000 observations,

Table 1. Summary of the full-factorial experimental design

Rake angle (A)	*Cutting speed (B)*	*Interaction (AB)*
-1	-1	$+1$
$+1$	-1	-1
-1	$+1$	-1
$+1$	$+1$	$+1$

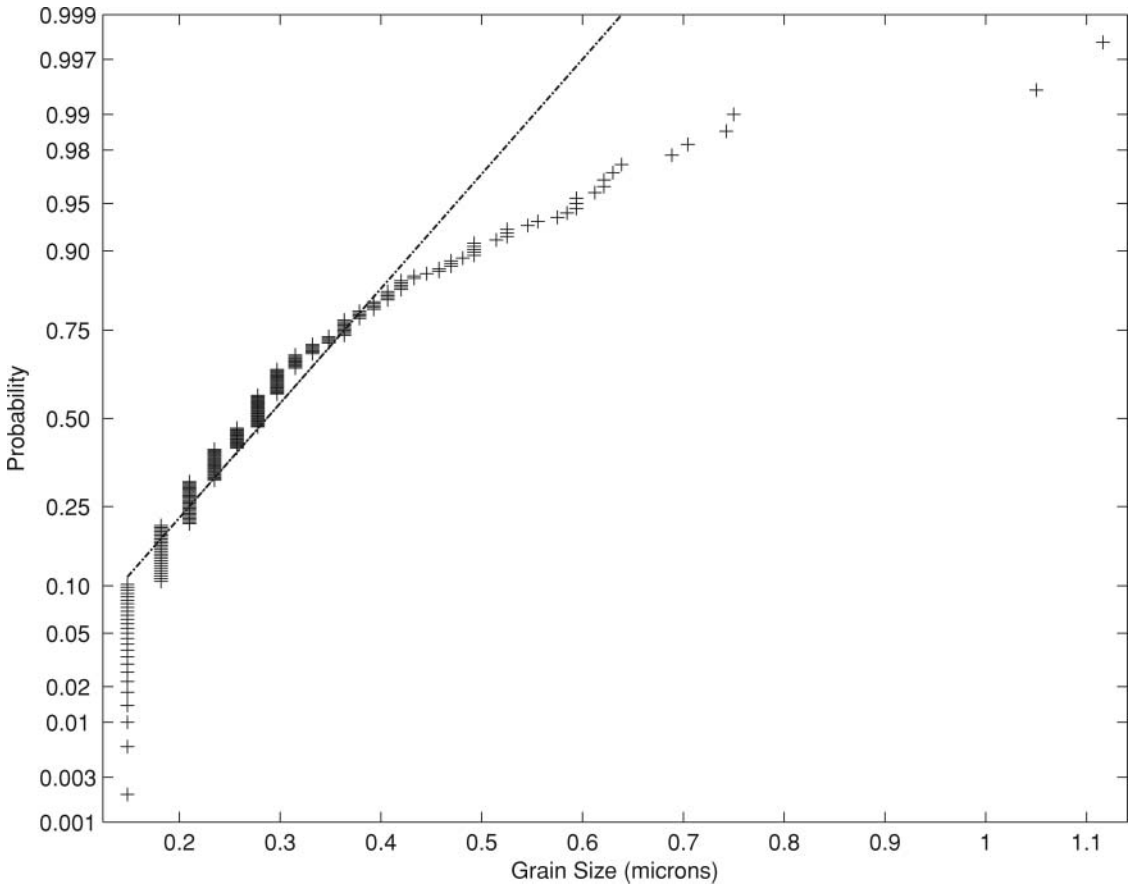

Fig. 4. Normal probability plot of grain size with A and B at their low levels.

we selected an equal number of grain size observations from each chip in order to facilitate balance in the design and to ease the computational burden. It is worth noting that additional observations at the grain level do not add benefit since the n_{ij} contribute to the estimation of σ_ϵ^2 and not σ_v^2.

The grain size distribution is typically highly right-skewed as indicated by the normal probability plot of Fig. 4 where the response data were taken from the $(-1, -1)$ treatment combination (i.e., A and B at the low levels). Responses obtained from the other treatment combinations yield similar plots and, as a result, a power transformation on the grain size observations is appropriate. Using the iterative approaches for ML and REML estimation discussed in Section 4, Fig. 5 shows a plot of the log-likelihood functions using ML and REML methods versus the transformation parameter θ. Note that $\hat{\theta} = -0.5$ maximizes both the full and restricted log-likelihood functions, suggesting that the appropriate transformation is the inverse square root. Figure 6 shows normal probability plots of the untransformed response data ($\theta = 1$), as well as the transformed response ($\theta = -0.5$), both taken when A and B are at their low levels. Similar results were obtained for the other treatment combinations. Notice that the transformed response data more closely follow a normal distribution.

Tables 2–4 summarize the results of the analysis using the standard, ML, and REML approaches, respectively, including the effect estimates, standard errors of the effect estimates, and values of the test statistics. Box–Cox transformations were used to estimate the transformation parameter for the standard analysis approach, and similar to the ML and REML methods, the estimate of θ was $\hat{\theta} = -0.5$. Notice in Tables 2–4 that the effect estimates are identical for all three approaches. This is a direct result of the equivalence of ordinary least squares and generalized least squares in estimating $\boldsymbol{\beta}$ when using a balanced and orthogonal two-level design (cf. Graybill (1976)); however, the standard errors of the effect estimates differ. Note that by using the standard analysis approach, the estimated standard errors of the effect estimates reported in Table 2 are seriously underestimated, resulting in a false inflation of the test statistics. As a consequence, factors that are not truly significant can be falsely deemed as highly significant contributors to variability.

The results reported for the ML and REML cases in Tables 3 and 4 suggest that cutting speed (B) is a highly

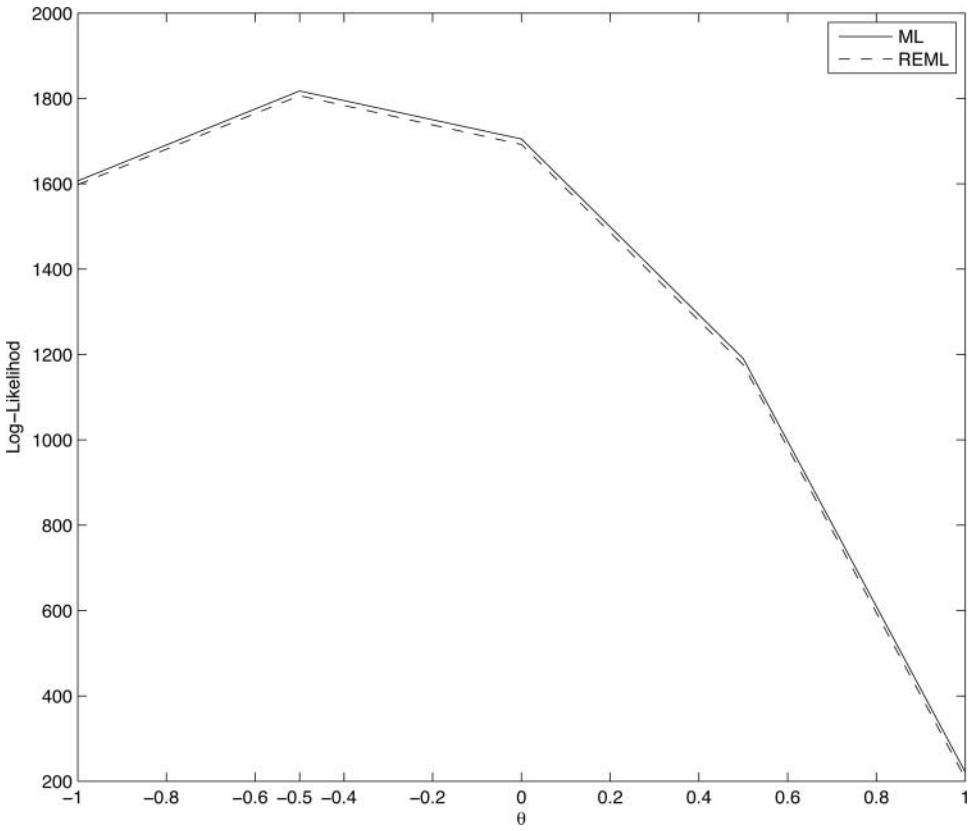

Fig. 5. ML and REML log-likelihood functions versus θ. Both methods produce $\hat{\theta} = -0.5$.

significant factor; however, the effects due to rake angle (A) and the interaction of rake angle and cutting speed (AB) may truly be null. If we base our decision on the standard normal distribution as the null distribution, then both A and AB are highly significant at the $\alpha = 0.05$ level of significance. For example, for the factor rake angle, the p-values corresponding to the ML and REML approaches are 0.0002 and 0.0055, respectively. For the interaction, the p-values corresponding to the ML and REML approaches are 0.0010 and 0.0148, respectively.

As an alternative, we used a simulation model to generate a large number of samples of the test statistic Z_0 given by Equation (18) under the null hypothesis H_0: $\beta_h = 0$ for both the ML and REML cases and then used the estimated percentiles of these distributions as critical values for the tests. Using two replicates of the design given in Table 1 with $n_{i1} = 250$ (for all i), as well as the ML and REML estimates for σ_v^2, σ_ϵ^2, and β_0 obtained from our analysis, we generated 10 000 samples and obtained the estimated percentiles displayed in Fig. 7.

The percentiles of the standard normal distribution are included in Fig. 7 as a frame of reference. Note that although the null distributions for each case have zero mean, the variances of the null distributions corresponding to the ML and REML approaches are much larger than that expected under the standard normal distribution.

In comparing the test statistics of Tables 3 and 4 to their corresponding null distributions given in Fig. 7, we see that both the ML and REML methods suggest that the only significant factor at the $\alpha = 0.05$ level of significance is

Table 2. Estimated effects and standard errors using standard methods

Source of variability	*Effect*	*Standard error*	Z_0
Rake angle (A)	0.1996	0.0172	11.5742
Cutting speed (B)	0.5226	0.0172	30.3126
Interaction (AB)	−0.1705	0.0172	−9.8920

Table 3. Estimated effects and standard errors using ML method

Source of variability	*Effect*	*Standard error*	Z_0
Rake angle (A)	0.1996	0.0554	3.6001
Cutting speed (B)	0.5226	0.0554	9.4285
Interaction (AB)	−0.1705	0.0554	−3.0768

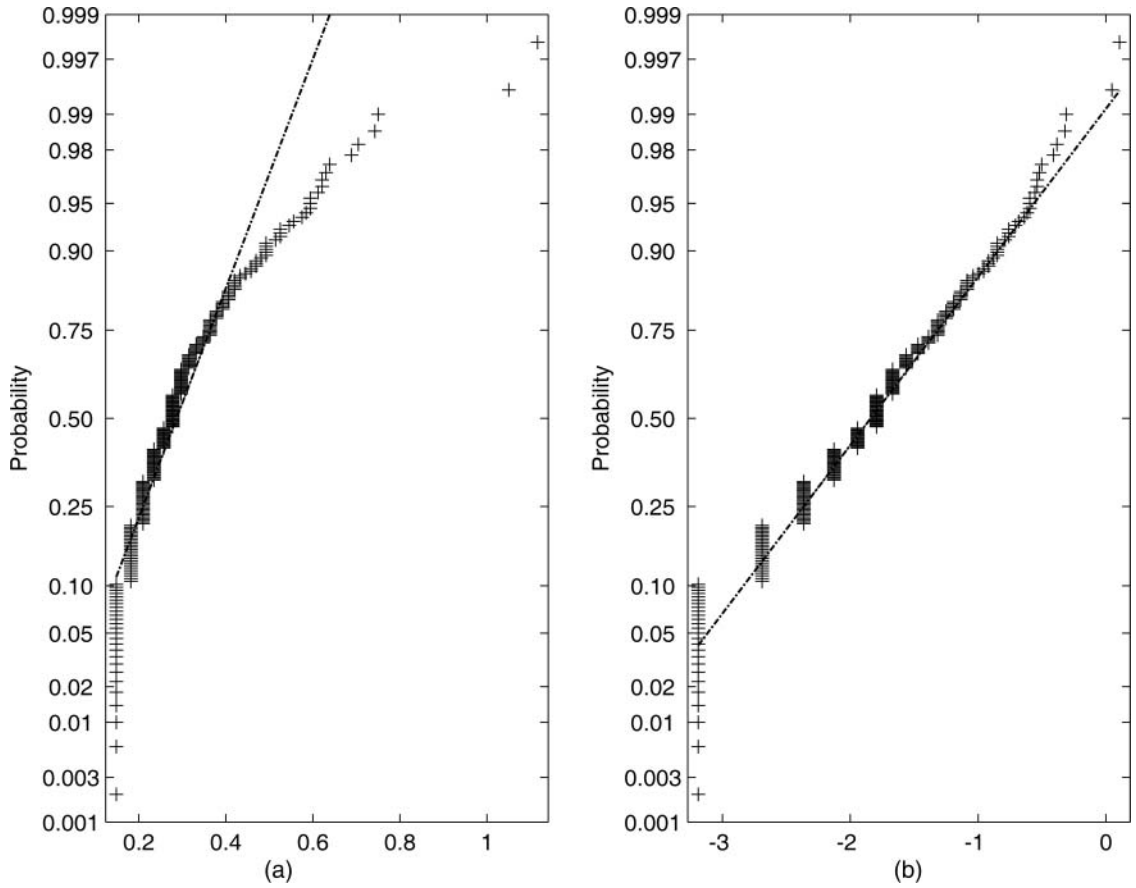

Fig. 6. Normal probability plots of grain size for (a) untransformed and (b) transformed data for Case 0L.

factor B, or cutting speed. From these experiments (using only two replications), there is not enough evidence to suggest that A or AB contribute significantly at the $\alpha = 0.05$ level. Figure 8 is the normal probability plot of the residuals obtained from the model of mean grain size in the transformed domain. Note that the fitted model produces residuals that appear to follow a zero-mean normal distribution. It was determined that the extreme residuals were due primarily to round-off error on the measured grain sizes.

Consequently, we have the following predictive model for the mean grain size as a function of factor B, or cutting speed:

$$\hat{y}(B) = -1.08 + 0.5226B, \tag{20}$$

where $\hat{y}(B)$ denotes the fitted value (in transformed units) as a function of cutting speed. Keeping in mind that this analysis was performed in transformed units, we need to transform the model back to the original units if it is to be

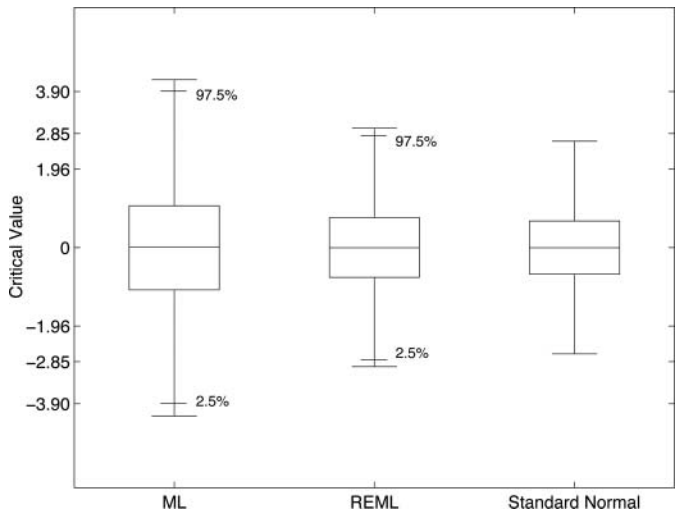

Fig. 7. Percentile points of null distributions.

Table 4. Estimated effects and standard errors using REML method

Source of variability	*Effect*	*Standard error*	Z_0
Rake angle (A)	0.1996	0.0784	2.5456
Cutting speed (B)	0.5226	0.0784	6.6670
Interaction (AB)	−0.1705	0.0784	−2.1757

useful for prediction purposes. It follows that:

$$\tilde{y}(B) = \exp\left(\frac{\ln(1+\hat{\theta}\,\hat{y}(B))}{\hat{\theta}}\right) = \exp\left(\frac{\ln(1.54-0.2613\,B)}{-0.5}\right), \qquad (21)$$

where $\tilde{y}(B)$ denotes the fitted value in the *original units* of the response (namely, micrometers) as a function of cutting speed. The argument of Equation (21) is the cutting speed B in coded units. Specifically, $B = -1$ corresponds to the low level (50 mm/s), and $B = 1$ corresponds to the high level (1250 mm/s). For intermediate cutting speeds between the factorial points, one can simply perform a linear interpolation between the two. For example, to predict the mean grain size when the cutting speed is at the midpoint 650 mm/s, substitute $B = 0$ in Equation (21). It is important to note that model (21) is intended to predict only the mean of the grain size distribution and does not prescribe the form of the distribution itself.

To demonstrate the efficacy of the mean grain size model as a function of only cutting speed, we compared estimates obtained from the fitted model in Equation (21) to sample estimates obtained from the empirical data with the cutting speed set at 50 mm/s ($B = -1$), 550 mm/s ($B = -0.1667$), and 1250 mm/s ($B = 1$). Figure 9 shows box plots of the measured grain sizes obtained from the validation runs taken at the low, medium, and high levels of cutting speed. Table 5 summarizes point estimates of mean grain size (in original units of micrometers), along with the actual sample mean grain size for each case. It is important to note that the sample statistics of Table 5 and Fig. 9 were obtained using observed grain sizes that are distinct from those observations used to create Model (21). For each level of cutting speed, the predicted value obtained from Equation (21) lies within the interquartile range of the validation data. The results suggest that the model is valid as the predicted and actual values in Table 5 are reasonably close. It is not surprising that there is greater discrepancy between the observed and predicted mean values at the high level of cutting speed. This discrepancy can possibly be attributed

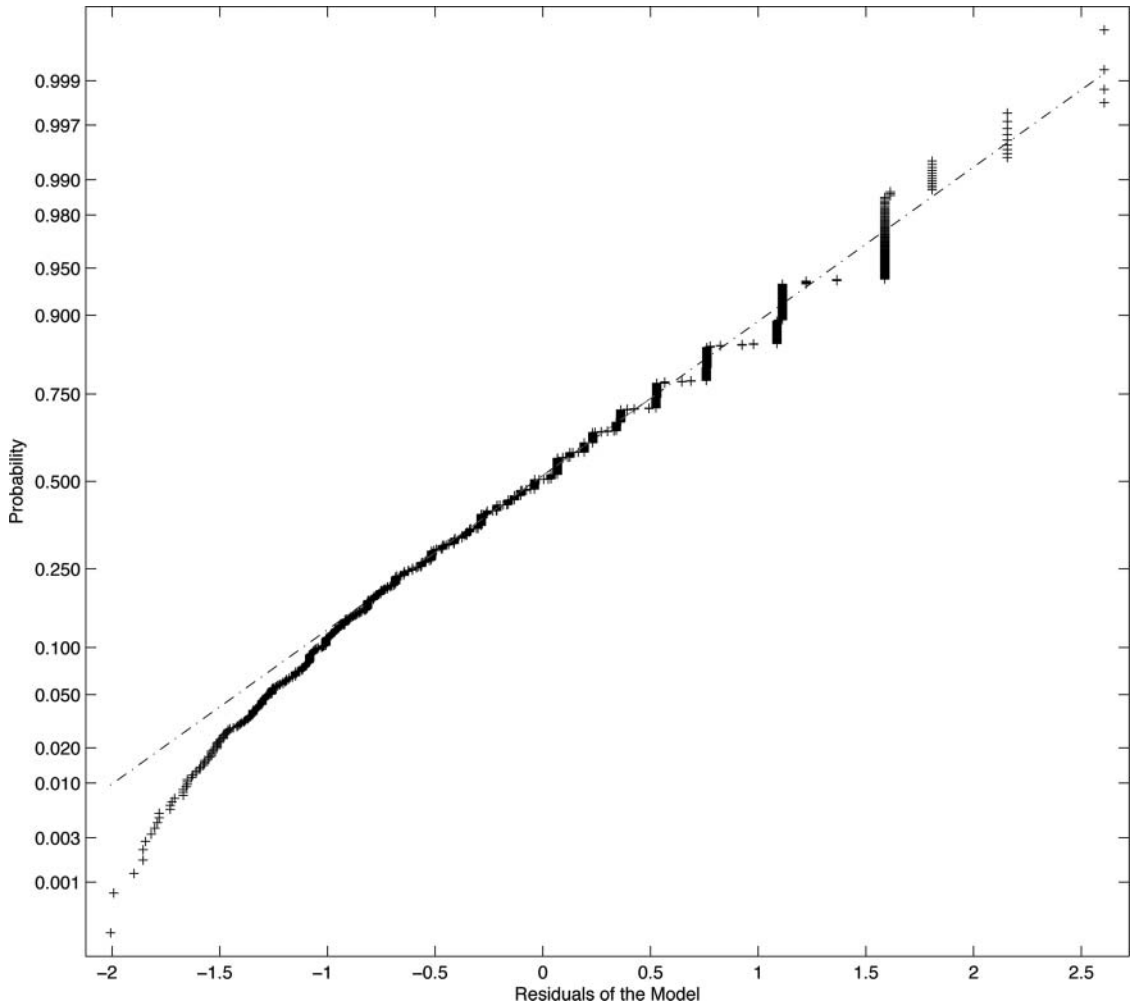

Fig. 8. Normal probability plot of the model residuals (transform domain).

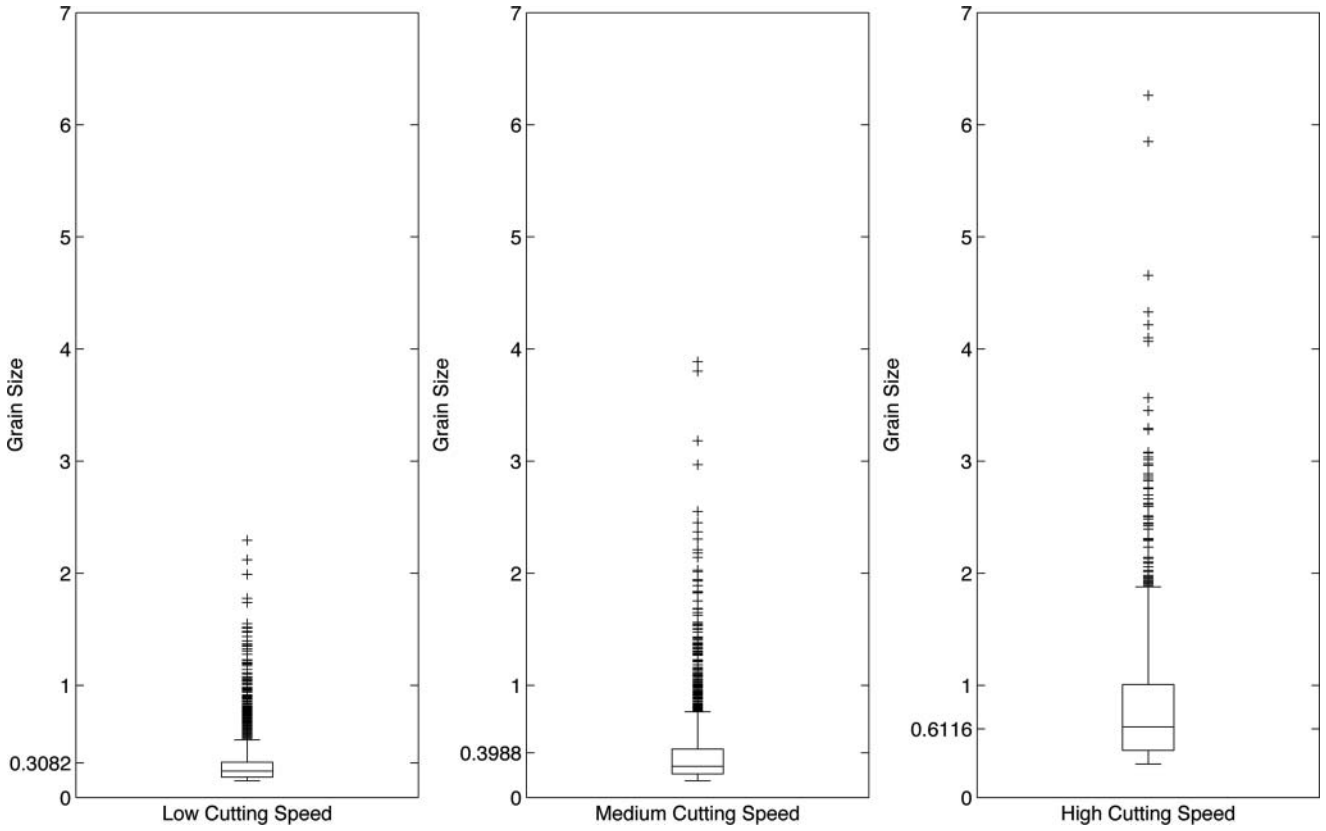

Fig. 9. Box plots of sampled grain sizes at various cutting speeds.

to an observed increase in the variance of the grain size distribution at the high cutting speed (see Fig. 9). That is, in addition to a significant *location* effect, cutting speed appears to have a significant *dispersion* effect that should not be ignored. These results may also indicate the need to include a second-order term for cutting speed in the model.

For the experiments detailed herein, our primary aim was to detect and estimate the main effects (A and B) and the two-factor interaction (AB); thus, the two-level factorial experiment is sufficient to fit the postulated model. However, in future experiments, we anticipate the need to estimate quadratic effects and, therefore, the analysis of second-order response surface designs will be required to establish the empirical mappings between experimental factors and surface microstructure. Fortunately, the model estimation methods outlined in this article are appropriate for estimating second and higher-order response surface models.

Table 5. Point estimates for mean grain size using validation data and associated percentiles

Cutting speed (mm/s)	*Sample mean (μm)*	*Sample percentiles*			*Predicted mean (μm)*
		25th	*50th*	*75th*	
50	0.2819	0.1819	0.2348	0.3150	0.3082
550	0.3836	0.2100	0.2778	0.4329	0.3988
1250	0.8265	0.4201	0.6301	1.0072	0.6116

6. Conclusions and future work

Emerging trajectories in engineering multifunctional surfaces have focused on utilizing nanoscale microstructures to achieve novel combinations of mechanical, biological, and electrochemical property responses. Recently, it was discovered that the SPD associated with machining-based processes can engender a novel interplay of thermomechanical phenomena to result in highly refined nanograined surfaces. However, to date, the detailed mappings between the parameters of machining and the resulting surface microstructures have remained obscured. This article has taken a first step toward the development of an empirically driven approach for the identification of significant machining factors and the estimation of important surface characteristics such as the mean size of nanostructured grains. Our numerical illustrations showed that significant variability stems from the cutting speed, and this variability has a significant impact on the measured average grain size. A more detailed model that incorporates second-order effects is likely needed; however, our aim here was to

emphasize the need for appropriate statistical techniques when analyzing these complex processes. The ability to introduce nanograin surfaces on bulk materials directly via machining-based processes, apart from physical, chemical, or mechanical treatments, has the potential to offer a scalable manufacturing framework for engineering novel surfaces within existing manufacturing paradigms.

Before such an approach can be realized, manufacturing engineers must first contend with the costly and time-consuming process of collecting and analyzing data originating from microscopy scans. In these experiments, non-normality and correlation of the grain size observations are prevalent due to the inherent nested error structure of experiments of this kind. Unfortunately, it is still common in practice to apply standard analysis methods (e.g., ANOVA or standard regression techniques) to analyze experimental data with nested error structures. By ignoring the inherent dependence of the grain size observations, the impact of the fixed effects on the mean grain size can be grossly misrepresented. The model we have presented here provides an appropriate way to analyze data originating from experiments of this type. Moreover, it lays a foundation for a framework to establish empirical mappings between important machining conditions and multiple response characteristics (e.g., the mean, dispersion, and skewness of the grain size distribution) that can be used to elucidate the effects of important machining parameters on the resulting surface microstructure.

Our statistical characterization framework may be applicable to an array of other materials science problems where the distribution of microstructural characteristics modify, adversely or favorably, the overall material response. One example is the characterization of second phases in metal matrix composites where the "clumping" of reinforcing particles surrounded by the metallic phase is known to unexpectedly modify the resulting mechanical behavior. A second example is in the characterization of metallic nanoparticles that are manufactured using chemical methods or gas-phase condensation techniques wherein their coarsening behavior and thermodynamic stability is a function of their size distributions. For such problems, a designed experiments approach can offer a powerful solution for capturing critical divergences that may not be otherwise resolved using conventional characterizations.

Acknowledgements

The authors are grateful to three anonymous referees and Professor Satish Bukkapatnam for helpful comments that have improved the content and presentation of this work. M.R. Shankar acknowledges support from the National Science Foundation (CMMI-0826010, CMMI-0856626, and CMMI-0927410) and the Nuclear Regulatory Commission (Faculty Development Grant). The authors also thank the Department of Mechanical Engineering and Materials Science at the University of Pittsburgh for providing access to the electron microscopy instrumentation and for assistance with the execution of this component of our research.

References

Al-Ostaz, A., Diwakar, A. and Alzebdeh, K.I. (2007) Statistical model for characterizing random microstructure of inclusion-matrix composites. *Journal of Materials Science*, **42**, 7016–7030.

Box, G.E.P. and Cox, D.R. (1964) An analysis of transformations. *Journal of the Royal Statistical Society* B, **26**, 211–243.

Box, G.E.P. and Jones, S.P. (1992) Split-plot designs for robust product experimentation, *Journal of Applied Statistics*, **19**, 3–26.

Cai, J., Shekhar, S., Wang, J. and Shankar M.R. (2009) Nano-twinned microstructures from low stacking fault energy brass by high-rate severe plastic deformation. *Scripta Materialia*, **60**, 599–602.

Calistes, R., Swaminathan, S., Murthy, T.G., Huang, C., Saldana, C., Shankar, M.R. and Chandrasekar, S. (2009) Controlling gradation of severe surface strains and nanostructuring by large strain machining. *Scripta Materialia*, **60**, 17–20.

Corbeil, R.R. and Searle, S.R. (1976) Restricted maximum likelihood (REML) estimation of variance components in the mixed model. *Technometrics*, **18**, 31–38.

Di Schino, A., Barteri, M. and Kenny, J.M. (2003) Grain size dependence of mechanical, corrosion and tribological properties of high nitrogen stainless steels. *Journal of Materials Science*, **38**, 3257–3262.

Graybill, F.A. (1976) *Theory and Application of the Linear Model*, Duxbury, North Scituate, MA.

Grosselle, F., Timeeli, G. and Bonollo, F. (2010) DOE applied to microstructural and mechanical properties of Al-Si-Cu-Mg casting alloys for automotive applications. *Materials Science and Engineering A*, **527**, 3536–3545.

Gurka, M.J., Edwards, L.J., Muller, K.E., and Kupper, L.L. (2006) Extending the Box–Cox transformations to the linear mixed model. *Journal of the Royal Statistical Society A*, **169**, 273–278.

Hartley, H.O. and Rao, J.N.K. (1967) Maximum-likelihood estimation for the mixed analysis of variance model. *Biometrika*, **54**(1–2), 93–108.

Harville, D.A. (1977) Maximum likelihood approaches to variance component estimation and to related problems. *Journal of the American Statistical Association*, **72**(358), 320–338.

Hocking, R.R. (2003) *Methods and Applications of Linear Models: Regression and the Analysis of Variance*, John Wiley & Sons, New York, NY.

Hofler, H.J., Averback, R.S., Hahn, H. and Gleiter, H. (1993) Diffusion of bismuth and gold in nanocrystalline copper. *Journal of Applied Physics*, **74**, 3382–3389.

Horvath, J. (1990) Diffusion in nanocrystalline materials, in *Defect and Diffusion Forum*, Kedves, F.J. and Beke, D.L. (eds), Trans Tech S.A., Zurich, Switzerland, pp. 207–228.

Huang, C., Murthy, T.G., Shankar, M.R., M'Saoubi, R. and Chandrasekar, S. (2008) Temperature rise in severe plastic deformation of titanium at small strain rates. *Scripta Materialia* **58**(8), 663–666.

Iglesias, P., Bermudez, M.D., Moscoso, W., Rao, B.C., Shankar, M.R. and Chandrasekar, S. (2007) Friction and wear of nanostructured metals created by large strain extrusion. *Machining Wear*, **263**, 636–642.

Kempthorne, O. (1952) *The Design and Analysis of Experiments*, John Wiley & Sons, New York, NY.

Kenward, M.G. and Roger, J.H. (1997) Small sample inference for fixed effects from restricted maximum likelihood. *Biometrics*, **53**(3), 983–997.

Mishra, R. and Balasubramaniam, R. (2004) Effect of nanocrystalline grain size on the electrochemical and corrosion behavior of nickel. *Corrosion Science*, **46**, 3019–3029.

Misra, R.D.K., Thein-Han, W.-W., Pesacreta, T.C., Hasenstein, K.H., Somani, M.C. and Karjalainen, L.P. (2009a) Cellular response of preosteoblasts to nanograined/ultrafine-grained structures. *Acta Biomaterialia*, **5**, 1455–1467.

Misra, R.D.K., Thein-Han, W.-W., Pesacreta, T.C., Hasenstein, K.H., Somani, M.C. and Karjalainen, L.P. (2009b) Favorable modulation of pre-osteoblast response to nanograined/ultrafine-grained structures in austenitic stainless steel. *Advanced Materials*, **21**, 1280–1285.

Montgomery, D.C. (2009) *Design and Analysis of Experiments*, John Wiley & Sons, New York, NY.

Nelson, L.S. (1985) What do low *F* ratios tell you? *Journal of Quality Technology*, **17**, 237–238.

op't Hoog, C., Birbilis, N. and Estrin, Y. (2008) Corrosion of Pure Mg as a function of grain size and processing route. *Advanced Engineering Materials*, **10**, 579–582.

Patterson, H.D. and Thompson, R. (1971) Recovery of inter-block information when block sizes are unequal. *Biometrika*, **58**(3), 545–554.

Raman, R.K.S. and Gupta, R.K. (2009) Oxidation resistance of nanocrystalline vis-à-vis microcrystalline Fe-Cr alloys. *Corrosion Science*, **51**, 316–321.

Roland, T., Retraint, D., Lu, K. and Lu, J. (2006) Fatigue life improvement through surface nanostructuring of stainless steel by means of surface mechanical attrition treatment. *Scripta Materialia*, **54**, 1949–1954.

Satterthwaite, F.F. (1941) Synthesis of variance. *Psychometrika* **6**, 309–316.

Sevier, M., Lee, S., Shankar, M.R., Yang, H.T.Y., Chandrasekar, S. and Compton, W.D. (2006) Deformation mechanics associated with formation of ultra-fine grained chips in machining. *Materials Science Forum*, **503–504**, 379–384.

Shankar, M.R., Chandrasekar, S., King, A.H. and Compton, W.D. (2005) Microstructure and stability of nanocrystalline aluminum 6061 created by large strain machining. *Acta Materialia*, **53**, 4781–4793.

Shankar, M.R.. Rao, B.C., Chandrasekar, S., Compton, W.D. and King, A.H. (2008) Thermally stable nanostructured materials from severe plastic deformation of precipitation-treatable Ni-based alloys. *Scripta Materialia*, **58**, 675–678.

Shankar, M.R., Rao, B.C., Lee, S., Chandrasekar, S., King, A.H. and Compton, W.D. (2006) Severe plastic deformation (SPD) of titanium at near-ambient temperature. *Acta Materialia*, **54**, 3691–3700.

Shankar, M.R., Verma, R., Rao, B.C., Chandrasekar, S., Compton, W.D., King, A.H. and Trumble, K.P. (2007) Severe plastic deformation of difficult-to-deform materials at near-ambiten temperatures. *Metallurgical and Materials Transactions A*, **38**, 1899–1905.

Shaw, M.C. (1984) *Metal Cutting Principles*, Clarendon Press, Oxford, UK.

Shekhar, S., Cai, J., Basu, S., Abolghasem, S. and Shankar, M.R. (2011) Effect of strain-rate in severe plastic deformation on microstructure refinement and stored energies. *Journal of Materials Research*, **26**, 395–406.

Shekhar, S., Cai, J., Wang, J. and Shankar, M.R. (2009) Multimodal ultrafine grain size distribution from severe plastic deformation at high strain rates. *Materials Science and Engineering: A* **527**, 187–191.

Shi, Y.N. and Han, Z. (2008) Tribological behaviors of nanostructured surface layer processed by means of surface mechanical attrition treatment. *Key Engineering Materials*, **384**, 321–334.

Silverman, B.W. (1986) *Density Estimation for Statistics and Data Analysis*, Chapman and Hall, London, UK.

Tao, K., Choo, H., Li, H., Clausen, B., Jin, J. and Lee, Y. (2007) Transformation-induced plasticity in an ultrafine-grained steel: an *in situ* neutron diffraction study, *Applied Physics Letters*, **90**, 101911-1–101911-3.

Tao, N., Tong, W., Wang, Z., Wang, W., Sui, M., Lu, J. and Lu, K. (2003) Mechanical and wear properties of nanostructured surface layer in iron induced by severe mechanical attrition treatment. *Journal of Materials Science and Technology*, **19**, 563–566.

Torquato, S. (2002) Statistical description of microstructures. *Annual Review of Materials Research*, **32**, 77–111.

Valiev, R.Z., Alexandrov, I.V., Zhu, Y.T. and Lowe, T.C. (2002) Paradox of strength and ductility in metals processed by severe plastic deformation. *Journal of Materials Research*, **17**, 5–8.

Valiev, R.Z., Islamgaliev, R.K. and Alexandrov, I.V. (2000) Bulk nanostructured materials from severe plastic deformation. *Progress in Materials Science*, **45**(2), 103–189.

Valiev, R.Z., Zehetbauer, M.J., Estrin, Y., Hoppel, H.W., Ivanisenko, Y., Hahn, H., Wilde, G., Roven, H.J., Sauvage, X. and Langdon, T.G. (2007) The innovation potential of bulk nanostructured materials. *Advanced Engineering Materials*, **9**, 527–533.

Youngdahl, C.J., Weertman, J.R., Hugo, R.C. and Kung, H.H. (2001) Deformation behavior in nanocrystalline copper. *Scripta Materialia*, **44**, 1475–1478.

Zhang, Z.F., Wu, S.D., Li, Y.J., Liu, S.M. and Wang, Z.G. (2005) Cyclic deformation and fatigue properties of Al-0.7 wt.% Cu alloy produced by equal channel angular pressing. *Materials Science and Engineering A*, **412**, 279–286.

Biographies

Marcus B. Perry is an Assistant Professor of Statistics in the Department of Information Systems, Statistics, and Management Science at the University of Alabama in Tuscaloosa. His research interests include statistical process control, design and analysis of experiments, response surface methods, applied optimization, regression analysis, and quality control. He serves on the Editorial Boards of *Quality Engineering* and *Quality and Reliability Engineering International*. He is a professional member of IIE, ASQ, ASA, and INFORMS.

Jeffrey P. Kharoufeh is an Associate Professor in the Department of Industrial Engineering at the University of Pittsburgh. He holds a Ph.D. in Industrial Engineering and Operations Research from the Pennsylvania State University. His primary research interest is the modeling, analysis, and control of stochastic systems with applications in reliability, queueing, and communications systems. He is a Senior Member of IIE and a professional member of INFORMS and the Applied Probability Society.

Shashank Shekhar has recently joined the Indian Institute of Technology at Kanpur as an Assistant Professor. He was a Visiting Research Assistant Professor in the Department of Industrial Engineering at the University of Pittsburgh. He received his Bachelor of Technology degree in Metallurgical Engineering and Materials Science from the Indian Institute of Technology–Bombay. He holds a Ph.D. in Materials Science from Purdue University, West Lafayette.

Jiazhao Cai is a Ph.D. student in the Department of Industrial Engineering at the University of Pittsburgh. She received her B.S. and M.S. in Materials Science and Engineering from the Zhejiang University in China. Her Ph.D. research focuses on manufacture of ductile and thermally stable bulk nanomaterials.

M. Ravi Shankar is an Assistant Professor in the Department of Industrial Engineering at the University of Pittsburgh. He holds a Ph.D. in Industrial Engineering from Purdue University, West Lafayette. His research interests include modeling of manufacturing processes, engineering nanomaterials, and nanomechanics.